Acta Mech 224, 1901–1915 (2013)
DOI 10.1007/s00707-013-0853-y

R. Avazmohammadi · R. Naghdabadi

Effective behavior of porous elastomers containing aligned spheroidal voids

Received: 11 December 2012 / Revised: 8 March 2013 / Published online: 6 April 2013

Abstract The theoretical need to recognize the link between the basic microstructure of nonlinear porous materials and their macroscopic mechanical behavior is continuously rising owing to the existing engineering applications. In this regard, a semi-analytical homogenization model is proposed to establish an overall, continuum-level constitutive law for nonlinear elastic materials containing prolate/oblate spheroidal voids undergoing finite axisymmetric deformations. The microgeometry of the porous materials is taken to be *voided spheroid assemblage* consisting of confocally voided spheroids of all sizes having the same orientation. Following a kinematically admissible deformation field for a confocally voided spheroid, which is the basic constituent of the microstructure, we make use of an energy-averaging procedure to obtain a constitutive relation between the macroscopic nominal stress and deformation gradient. In this work, both prolate and oblate voids are considered. As a numerical example, we study macroscopic nominal stress components for a hyperelastic porous material consisting of a neo-Hookean matrix and prolate/oblate voids subjected to 3-D and plane strain dilatational loadings. In this numerical study, the relation between the relevant microstructural variables (i.e., initial porosity and void aspect ratio) for a rather large range of applied stretch is put into evidence for two types of loading. Finally, a finite element (FE) simulation is presented, and the homogenization model is assessed through comparison of its predictions with the corresponding FE results. The illustrated agreement between the results demonstrates a good accuracy of the model up to rather large deformations.

1 Introduction

Estimation of the overall mechanical response of random heterogeneous materials is of great interest to researchers from both scientific and engineering standpoints. A large number of homogenization models for determining effective stiffness moduli of linearly elastic heterogeneous solids have been proposed. A comprehensive review on this subject can be found in [1–3]. Recently, considerable attention has been directed toward developing similarly extensive treatments in the area of homogenization of nonlinear elastic heterogeneous solids undergoing finite deformations (see, for example, Refs. [4,5]). From an engineering point of view, the mechanical properties of elastomeric materials can be controlled by incorporation of well-defined modifier particles in a matrix [6]. A similar situation arises in the case of porous elastomeric materials, in

R. Avazmohammadi (✉)
Department of Mechanical Engineering and Applied Mechanics, University of Pennsylvania,
Philadelphia, PA 19104, USA
E-mail: rezaavaz@seas.upenn.edu

R. Naghdabadi
Department of Mechanical Engineering, Sharif University of Technology, Tehran, Iran

R. Naghdabadi
Institute for Nano Science and Technology, Sharif University of Technology, Tehran, Iran

which the pores are either formed unintentionally, such as defects, or introduced deliberately as a part of the manufacturing process [4]. In all of these situations, improved toughness/stiffness of elastomers may become a considerable factor of material selection in many structural applications [6].

One of the most notable approaches among the contributions to the homogenization of nonlinear composite/porous elastic solids is employing a variational procedure to obtain estimates (and possibly lower and upper bounds) for the effective behavior of solids. Among others, we mention the pioneering work of Talbot and Willis [7]. Also, second-order homogenization methods originally developed by Ponte Castañeda [8] for viscoplastic materials and extended later for hyperelastic composites by Lopez-Pamies and Ponte Castañeda [9] are well-known works in this approach. A common strategy within these nonlinear homogenization methods is constructing suitable minimum energy principles along with utilizing the technique of "comparison composites," which is defined by a suitable linearization of the constitutive behavior of the nonlinear phases. In this way, one will be able to generate macroscopic behavior for nonlinear composite/porous materials by building upon already available estimates for the corresponding "comparison composite".

Another way to predict the deformation behavior of heterogeneous solids at the macrolevel is solving suitably defined boundary value problems for a so-called representative volume element (RVE) of the solids and then use of a volume-averaging process over RVE [1]. In this context, the classical composite sphere assemblage (CSA) and composite cylinder assemblage (CCA) models, which, respectively, trace back to the papers by Hashin [10] and Hashin and Rosen [11], are the most well-known RVEs for two-phase composites with randomly distributed particles or fibers. In this microstructure, the whole space is filled by concentrically coated spherical (or cylindrical) elements of all sizes, while the volume fraction of all elements is the same. In addition, some contributions have been devoted to make use of the *composite sphere/cylinder assemblage* as RVEs in finite deformation context in order to deal with the overall mechanical behavior of elastomeric composites or *voided* elastomers; see for instance works by Hashin [12], Kakavas and Anifantis [13], Danielsson et al. [4], deBotton et al. [14], deBotton and Hariton [15], Avazmohammadi and Naghdabadi [16], Avazmohammadi et al. [17] and Goudarzi and Lopez-Pamies [18]. In this approach, a single *spherical/cylindrical composite element* subjected to the macroscopic deformation is examined. In particular, Danielsson et al. [4] obtained an overall constitutive law for elastomeric porous materials containing randomly distributed spherical voids by making use of a *kinematically admissible* deformation field for a hollow sphere under tri-axial stretching.

More general effective properties of heterogeneous solids are obtained, when an ellipsoidal shape is assigned to the inhomogeneities. In this connection, we choose the spheroidal shape for voids as it has been broadly employed in the theoretical studies as the model shape of dispersed pores. This choice is practical since the spheroidal shape allows us to represent within one unified model the variety of pores, including needlelike and disk cracks. Among the substantial literature on the elastic effective properties of solids with spheroidal pores in the context of *linear elasticity*, we mention the work of Zhao et al. [19] who used the Mori–Tanaka method. Also, as a rare study on the effective properties of porous solids with spheroidal pores in the context of *nonlinear elasticity*, Bouchart et al. [20] used the second-order homogenization and implemented a computational scheme to evaluate the macroscopic nominal stress.

The purpose of the present work is to develop a semi-analytic solution for obtaining the overall mechanical behavior of a nonlinear elastic porous solid consisting of a *transversely isotropic* distribution of prolate/oblate spheroidal voids in an incompressible matrix. The equivalent material (macrohomogeneous body) possesses the transverse isotropy by assuming that the matrix is isotropic. Only axisymmetric loadings with symmetry axis parallel to that of the voids are considered. Conventional volume-averaging technique is used to define the effective strain energy from which the effective nominal stress conjugating with the macroscopic deformation gradient tensor is derived. In order to assess the accuracy of the model, the predictions of analytic results for the overall nominal stress in the hydrostatic and plane strain loadings are compared to those of the finite element computations performed using an associated unit cell.

2 Representative volume element

The microstructure of porous (or composite) materials is idealized through the identification of a *representative volume element* of them. This idealization allows us to utilize analytical/ numerical tools to study a microstructure consisting of finite inhomogeneities randomly (or periodically) suspended in a matrix as a boundary value problem, in order to obtain both micro- and macro-level (RVE-average) information on stress and strain fields in the material. One of the well-known RVEs employed for the determination of overall properties is the *Composite Sphere Assemblage* (CSA) (see, e.g., Ref. [12]) whose building element is represented by a spherical

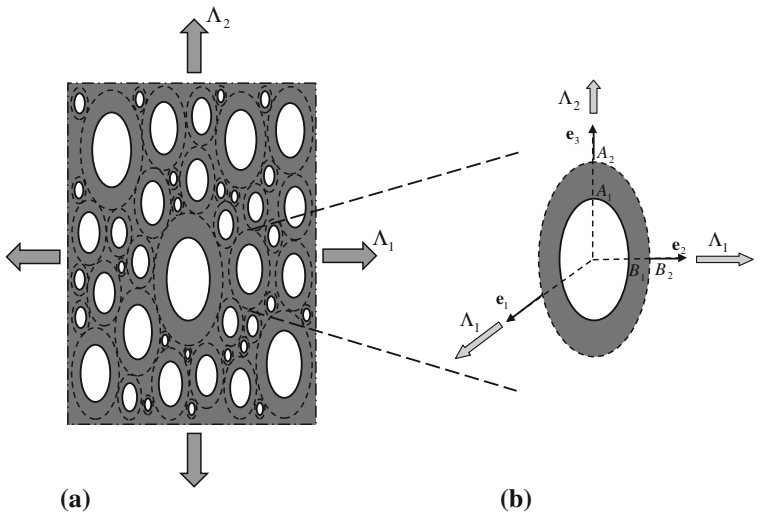

Fig. 1 Porous spheroids assemblage comprising of voided spheroidal elements undergoing tri-axial axisymmetric stretching

body consisting of a matrix surrounding a spherical inclusion. The generalization of CSA to the nonspherical inclusions falls within the category of the composite ellipsoid assemblages (CEA). In this microstructure, the whole space is filled by composite ellipsoidal elements of all sizes with the same (or random) orientation. The volume fractions of the ellipsoidal core (inclusion) and the confocal coating (matrix) are the same in all composite elements. A comprehensive review of the subject can be found in Chapters 7 and 8 of Ref. [2] and the paper by Benveniste and Milton [21].

In the present paper, we consider hyperelastic porous materials consisting of an incompressible matrix filled with unidirectionally aligned voids of spheroidal shape, subjected to an axisymmetric loading. We assume that the underlying microstructure can be represented by a (polydisperse) *Voided Spheroid Assemblage* which has been schematically shown in Fig. 1a (note that the cross lines denote the imaginary border of each voided spheroidal element). Making use of the principle of minimum potential energy together with a variational approximation (see Refs. [12,18]), the effective behavior of the assemblage can be approximated by that of a (confocally) voided spheroid, shown in Fig. 1b. Such a spheroidal volume element under applied stretch boundary conditions has been frequently employed in the literature to give a rigorous upper bound for the overall behavior of different porous materials, as we mention here works by Gologanu et al. [22,23] and Danielsson et al. [4].

3 Voided prolate spheroid subjected to a finite axisymmetric stretching

Here, we consider a prolate spheroidal void of major semi-axis A_1 and minor semi-axis B_1 surrounded by a confocal spheroidal matrix with major and minor semi-axes A_2 and B_2, respectively (see Fig. 1). Using the prolate spheroidal coordinate system, the reference configuration of the matrix phase is defined by

$$\Omega^P = \{(\Xi, H, \Theta) \in \mathbb{R}^3 : \Xi_1 \leq \Xi \leq \Xi_2, 0 \leq H < \pi, 0 \leq \Theta < 2\pi\}$$

where (Ξ, H, Θ) are the spheroidal material coordinates in the undeformed configuration, and superscript P refers to the parameters associated with the prolate spheroidal void throughout the formulation. Also, Ξ_1 and Ξ_2 are the outer spheroids of the void and matrix, respectively. With reference to the fixed Cartesian basis $\{\mathbf{e}_i\}$, we note that the spheroidal pores are initially aligned with the $\mathbf{e}_3$-axis. Also, the Cartesian components X_i can be written in terms of coordinates (Ξ, H, Θ) as

$$X_1 = C \sinh \Xi \sin H \cos \Theta, \quad X_2 = C \sinh \Xi \sin H \sin \Theta, \quad X_3 = C \cosh \Xi \cos H \tag{1}$$

where C is the distance from the origin to the foci of the spheroid on the $\mathbf{e}_3$-axis. However, because of the rotational symmetry of the problem considered here, it proves convenient to make use of polar cylindrical coordinates (R, Θ, Z) in the following form:

$$R = C \sinh \Xi \sin H, \quad \Theta = \Theta, \quad Z = C \cosh \Xi \cos H \tag{2}$$

where Z is the component in the $\mathbf{e}_3$-direction, and henceforth, unless stated, the components of any tensorial quantity will be referred to this coordinate system. The initial porosity, c_0, and the initial void aspect ratio, p, are given by $c_0 = B_1^2 A_1 / B_2^2 A_2$ and $p = A_1/B_1$, respectively.

In order to obtain the constitutive behavior of the porous material, a relation between the two macroscopic quantities, $\bar{\mathbf{S}}$, the macroscopic nominal stress tensor, and $\bar{\mathbf{F}}$, the macroscopic deformation gradient, should be developed. For our purposes in this work, we confine our attention to the macroscopic deformation gradient of the form

$$\bar{\mathbf{F}} = \mathrm{diag}(\Lambda_1, \Lambda_1, \Lambda_2) \tag{3}$$

where Λ_1 and Λ_2 are two constants. Under this deformation, the outer surface of the (*voided*) spheroid undergoes an axisymmetric stretching such that the location of the material points on the outer boundary in the deformed configuration is given by

$$r = \Lambda_1 R, \quad z = \Lambda_2 Z. \tag{4}$$

It is interesting to note that, under affine boundary conditions (4), the volume average of the deformation gradient over the voided spheroid is equal to $\bar{\mathbf{F}}$, given in (3). It is also remarked that in view of the above-described microstructure as well as the adopted macroscopic loading (4), the porous material remains a (macroscopically) transversely isotropic material for all deformations.

3.1 Deformation field

Determining an exact analytical solution for the local deformation field in the voided spheroid is a very difficult task, due to associated mathematical complexities. Therefore, we adopt an approximate solution by considering a particular class of kinematically admissible deformation field employed by Hou and Abeyaratne [24] and Danielson et al. [4] for a hollow sphere and by Gologanu et al. [22,23] for a hollow spheroid. In general, for the matrix of a voided ellipsoid undergoing tri-axial stretching at the outer boundary, this field relies on the assumption that all points on each ellipsoid in the undeformed configuration are mapped to corresponding points on another, generally nonconfocal, ellipsoid in the deformed configuration. This deformation for an axisymmetric loading in polar coordinates can be written as

$$r = \Phi_1^P(\Xi) R, \quad z = \Phi_2^P(\Xi) Z \tag{5}$$

where boundary conditions (4) at outer spheroidal surface of the voided element require that

$$\Phi_1^P(\Xi_2) = \Lambda_1, \quad \Phi_2^P(\Xi_2) = \Lambda_2. \tag{6}$$

The components of the deformation gradient associated with the deformation field (5) in cylindrical coordinates are given by

$$\mathbf{F}^{(1)} = \begin{pmatrix} \Phi_1^P + \frac{A \sin H}{D} R (\Phi_1^P)' & 0 & \frac{B \cos H}{D} R (\Phi_1^P)' \\ 0 & \Phi_1^P & 0 \\ \frac{A \sin H}{D} Z (\Phi_2^P)' & 0 & \Phi_2^P + \frac{B \cos H}{D} Z (\Phi_2^P)' \end{pmatrix} \tag{7}$$

where, here and elsewhere, $\Phi_i^P = \Phi_i^P(\Xi)$; $i = 1, 2$, the prime sign denotes differentiation with respect to Ξ, and superscript (1) refers to the variables associated with the matrix phase. In Eq. (7), use has been made of the relations

$$\frac{D(\Xi, H)}{D(R, Z)} \equiv \begin{bmatrix} \partial \Xi / \partial R & \partial \Xi / \partial Z \\ \partial H / \partial R & \partial H / \partial Z \end{bmatrix} = \frac{1}{D} \begin{bmatrix} A \sin(H) & B \cos(H) \\ B \cos(H) & -A \sin(H) \end{bmatrix} \tag{8}$$

where A, B and D are defined by

$$A = C \cosh \Xi, \; B = C \sinh \Xi \quad \textit{and} \quad D = A^2 \sin^2 H + B^2 \cos^2 H. \tag{9}$$

The incompressibility constraint in the matrix phase which requires

$$\det(\mathbf{F}^{(1)}) = 1 \tag{10}$$

can be applied to Eq. (7) to result in the following first-order ODE:

$$(\Phi_1^P)^2\Phi_2^P + \frac{AB\Phi_1^P}{D}[\Phi_1^P(\Phi_2^P)'\cos^2(H) + \Phi_2^P(\Phi_1^P)'\sin^2(H)] = 0. \tag{11}$$

Using the identity $\cos^2(H) = 1-\sin^2(H)$ and identifying terms independent of H and proportional to $\sin^2(H)$ (since the above equation must hold for every H), we obtain the following system of equations:

$$\begin{cases} \Phi_1^P(\Phi_2^P)' - \tanh^2(\Xi)(\Phi_1^P)'\Phi_2^P = 0, & (12.1)\\ (\Phi_1^P)^2\Phi_2 + \tanh(\Xi)(\Phi_1^P)'\Phi_1^P\Phi_2^P - 1 = 0. & (12.2) \end{cases}$$

First, by combining (12.1) and (12.2), one can obtain

$$(\Phi_1^P)^2 = \frac{\tanh(\Xi)}{\Phi_2^P\tanh(\Xi) + (\Phi_2^P)'} = \Omega^P(\Xi), \qquad 2\Phi_1^P(\Phi_1^P)' = [\Omega^P(\Xi)]'. \tag{13}$$

Then, by making use of (13) and replacing $(\Phi_1^P)^2$ and $(\Phi_1^P)'$ in (12.2) by equal Φ_2^P terms, it yields

$$2[(\Phi_2^P)']^2 + \tanh(\Xi)\Phi_2^P\{[1+2\tanh^2(\Xi)](\Phi_2^P)' + \tanh(\Xi)(\Phi_2^P)''\} = 0. \tag{14}$$

Upon letting $\Psi^P(\Xi) = \Phi_2^P/(\Phi_2^P)'$, Eq. (14) leads readily to the linear differential equation

$$[\Psi^P(\Xi)]' - [\coth^2(\Xi) + 2]\tanh(\Xi)\Psi^P(\Xi) - 2\coth^2(\Xi) - 1 = 0. \tag{15}$$

Equation (15) is integrated to give that

$$\Psi^P(\Xi) = \coth(\Xi)[C_1\cosh(\Xi)\sinh^2(\Xi) - 1], \tag{16}$$

where C_1 is an arbitrary constant. Next, making use of $\Psi^P(\Xi) = \Phi_2^P/(\Phi_2^P)'$ in (16), after some algebra, it yields

$$\Phi_2^P(\Xi) = C_2\mathrm{sech}(\Xi)\Upsilon_P, \quad \text{where } \Upsilon_P = \prod_{i=1}^{3}(\cosh(\Xi) - \delta_i^P)^{\frac{(\delta_i^P)^2-1}{3(\delta_i^P)^2-1}}. \tag{17}$$

Finally, on using (13), the function $\Phi_1^P(\Xi)$ can be written as

$$\Phi_1^P(\Xi) = \mathrm{cosech}(\Xi)\left[\frac{C_1\cosh(\Xi)\sinh^2(\Xi) - 1}{C_1C_2\Upsilon_P}\right]^{\frac{1}{2}}, \tag{18}$$

where C_1 and C_2 are integration constants, and δ_i^P; $i = 1, 2, 3$ are the three roots of the cubic equation $C_1(\delta^P)^3 - C_1\delta^P - 1 = 0$, given by

$$\begin{aligned} \delta_1^P &= (\sqrt[3]{12}\Gamma_P^2 + 2\sqrt[3]{18}C_1^2)/(6C_1\Gamma_P),\\ \delta_2^P &= [(\sqrt{3}i-1)\sqrt[3]{12}\Gamma_P^2 - 2\sqrt[3]{18}(\sqrt{3}i+1)C_1^2]/(12C_1\Gamma_P),\\ \delta_3^P &= -[(\sqrt{3}i+1)\sqrt[3]{12}\Gamma_P^2 - 2\sqrt[3]{18}(\sqrt{3}i-1)C_1^2]/(12C_1\Gamma_P) \end{aligned} \tag{19}$$

where $\Gamma_P = \left\{\left[9 + \sqrt{3(27-4C_1^2)}\right]C_1^2\right\}^{\frac{1}{3}}$, and $i = \sqrt{-1}$. The constants C_1 and C_2 should be determined using Eq. (6), which are strongly nonlinear algebraic equations and may be solved by the Newton–Raphson method.

4 The overall elastic constitutive law

Assuming that the local constitutive behavior of the porous material is characterized by means of the hyperelasticity theory, a strain density function $W^{(1)}$ is assigned to the (isotropic) matrix phase which is a function of deformation gradients $\mathbf{F}$. The strain energy for the matrix is assumed to have the functional form $W^{(1)} = W^{(1)}(I_1, I_2)$ due to the incompressibility constraint, in which the principal invariants I_j; $j = 1, 2, 3$ are defined by

$$I_1 = tr(\mathbf{C}), \qquad I_2 = \frac{1}{2}\{(I_1)^2 - tr[(\mathbf{C})^2]\}, \qquad I_3 = \det(\mathbf{C}) = 1 \tag{20}$$

where $\mathbf{C} = (\mathbf{F})^{\mathrm{T}}\mathbf{F}$ is the right Cauchy-Green tensor. Furthermore, admitting that the porous material macroscopically behaves like a hyperelastic one, we seek an, generally anisotropic, *effective strain energy function*, denoted by $\overline{W}$, for the equivalent homogeneous material. This quantity may be obtained by the volume average process, expressed by

$$\overline{W} = \frac{1}{V_0}\int_{V^{(1)}} W^{(1)}(I_1, I_2)dV \tag{21}$$

where V_0 and $V^{(1)}$ are the volumes occupied in the undeformed configuration by the hollow spheroid and matrix phase, respectively.

Following Hill [25], $\overline{W}$ is a function only of the average deformation gradient, $\overline{\mathbf{F}}$, provided that the same boundary conditions, specified on the RVE, produce uniform deformation and nominal stress throughout the equivalent homogeneous body, as is the case here. Therefore, the constitutive law for the overall behavior of the material is given by

$$\overline{\mathbf{S}} = \frac{\partial \overline{W}}{\partial \overline{\mathbf{F}}} \tag{22}$$

where $\overline{\mathbf{S}}$ is the *average nominal stress* for the porous material.

In the present work, the volume integral representation in Eq. (21) can be transformed into prolate spheroidal coordinates expressed as

$$\overline{W}^P = \frac{2\pi}{V_0}\int_{\Xi_1}^{\Xi_2}\int_0^{\pi} W^{(1)} J^P \mathrm{d}H\,\mathrm{d}\Xi = \int_{\Xi_1}^{\Xi_2} W^{*P}\mathrm{d}\Xi \tag{23}$$

where W^{*P} is the result of integrating $2\pi W^{(1)} J^P / V_0$ over H, while Ξ is treated as constant, and J^P stands for the *Jacobian* of the prolate spheroidal coordinate given by

$$J^P = \det\left(\frac{\partial(R, \Theta, Z)}{\partial(\Xi, \Theta, \mathrm{H})}\right) = \frac{C^3}{2}\sinh(\Xi)\sin(H)[\cosh(2\Xi) - \cos(2H)]. \tag{24}$$

Utilizing the equations $\Xi_1 = \coth^{-1}(p)$ and $\Xi_2 = \coth^{-1}(t^P)$, the effective strain energy $\bar{W}^P$ can be expressed as a function of the matrix material constants, Λ_1, Λ_2, p and c_0, in which $t^P = \sqrt{Y^P(p^2-1)+1}$ and Y^P is an acceptable root of the algebraic equation $(Y^P)^3 - (c_0/p)^2(p^2-1)Y^P - (c_0/p)^2 = 0$.

As the final step in the homogenization procedure, the macroscopic (average) nominal stress tensor $\overline{\mathbf{S}}$ conjugated with the macroscopic deformation gradient $\overline{\mathbf{F}}$ can be readily calculated by Eq. (22). It is remarked that the effective energy $\overline{W}$ belongs to the class of strain energy functions for transversely isotropic materials, and accordingly, the constitutive law (22) should be defined for this group of symmetry. Also, since this energy has been obtained as a function of two deformation invariants, Λ_1 and Λ_2, it is convenient to employ the constitutive behaviors of transversely isotropic materials for such invariant set developed by Criscione et al. [26] and deBotton et al. [14]. Accordingly, the macroscopic constitutive law is determined by

$$\overline{\mathbf{S}} = \frac{\partial \overline{W}}{\partial \overline{\mathbf{F}}} = \sum_{j=1}^{2}\frac{\partial \overline{W}}{\partial \Lambda_j^2}\frac{\partial \Lambda_j^2}{\partial \overline{\mathbf{F}}} = \sum_{j=1}^{2}\overline{W}_j\frac{\partial \Lambda_j^2}{\partial \overline{\mathbf{F}}} \tag{25}$$

where the explicit forms of kinematic tensors $\partial\Lambda_i^2/\partial\overline{\mathbf{F}}(i=1,2)$ for transversely isotropic materials are [14]

$$\frac{\partial\Lambda_1^2}{\partial\overline{\mathbf{F}}} = \Lambda_1^2\overline{\mathbf{F}}^{-T} - \frac{\Lambda_1^2}{\Lambda_2^2}\overline{\mathbf{F}}\mathbf{N}\otimes\mathbf{N}, \tag{26}$$

$$\frac{\partial\Lambda_2^2}{\partial\overline{\mathbf{F}}} = 2\overline{\mathbf{F}}\mathbf{N}\otimes\mathbf{N} \tag{27}$$

where $\mathbf{N}=\mathbf{e}_3$ denotes the initial orientation of spheroidal voids. Substituting Eqs. (26) and (27) into Eq. (25), the macroscopic nominal stress tensor $\overline{\mathbf{S}}$ is given by

$$\overline{\mathbf{S}} = \mathrm{diag}(\overline{W}_1\Lambda_1, \overline{W}_1\Lambda_1, 2\overline{W}_2\Lambda_2). \tag{28}$$

In addition, the macroscopic Cauchy stress $\overline{\mathbf{T}}$ is obtained as $\overline{\mathbf{T}} = (1/\overline{J})\overline{\mathbf{F}}\,\overline{\mathbf{S}}$.

Furthermore, due to mathematical complications associated with obtaining constants C_1 and C_2 (in Eqs. (17) and (18)) in explicit terms of Λ_1 and Λ_2, the scalar partial derivatives $\partial\overline{W}/\partial\Lambda_i^2$ are calculated as follows:

$$\overline{\mathrm{W}}_i = \frac{\partial\overline{W}}{\partial\Lambda_i^2} = \frac{1}{2\Lambda_i}\frac{\partial\overline{W}}{\partial\Lambda_i} = \frac{1}{2\Lambda_i}\sum_{j=1}^{2}\frac{\partial\overline{W}}{\partial C_j}\frac{\partial C_j}{\partial\Lambda_i}; \qquad i=1,2\ (\text{no sum}). \tag{29}$$

Now, the following set of equations is set up and solved by a Newton–Raphson scheme to determine the derivatives $\partial C_j/\partial\Lambda_i$ for given values of Λ_1 and Λ_2

$$\sum_{i=1}^{2}\frac{\partial\Phi_j(\Xi_2)}{\partial C_i}\frac{\partial C_i}{\partial\Lambda_k} = \frac{\partial\Lambda_j}{\partial\Lambda_k}; \qquad j,k=1,2. \tag{30}$$

5 Oblate spheroidal voids

The procedure of mathematical calculation in this case follows a similar course to the foregoing. Let us employ again the same symbols used in Sect. 3. It is assumed that A_1 and B_1 represent the minor and major semi-axes of the spheroidal void, respectively, surrounded by a confocal spheroidal matrix with minor and major semi-axes A_2 and B_2, respectively. Using the oblate spheroidal coordinate systems, the reference configuration of the matrix phase is defined by

$$\Omega^O = \{(\Xi, H, \Theta)\in\mathbb{R}^3 : \Xi_1\le\Xi\le\Xi_2, -\pi/2\le H<\pi/2, 0\le\Theta<2\pi\} \tag{31}$$

where, here and in what follows, the superscript O refers to the parameters associated with the porous material with oblate spheroidal voids. The relation between axisymmetric cylindrical coordinates (R, Z) and oblate spheroidal ones (Ξ, H) is given by

$$R = C\cosh\Xi\cos H,\ Z = C\sinh\Xi\sin H. \tag{32}$$

Similar to Eqs. (5) and (6), the kinematically admissible deformation field in the matrix is given by

$$r = \Phi_1^O(\Xi)R, \quad z = \Phi_2^O(\Xi)Z \tag{33}$$

which is subjected to the following boundary conditions:

$$\Phi_1^O(\Xi_2) = \Lambda_1, \qquad \Phi_2^O(\Xi_2) = \Lambda_2. \tag{34}$$

From (33), a routine calculation gives the components of the deformation gradient $\mathbf{F}^{(1)}$ as

$$\mathbf{F}^{(1)} = \begin{pmatrix} \Phi_1^O + \frac{B\cos H}{D}R(\Phi_1^O)' & 0 & \frac{A\sin H}{D}R(\Phi_1^O)' \\ 0 & \Phi_1^O & 0 \\ \frac{B\cos H}{D}Z(\Phi_2^O)' & 0 & \Phi_2^O + \frac{A\sin H}{D}Z(\Phi_2^O)' \end{pmatrix}. \tag{35}$$

In Eq. (35), we have made use of the relations

$$\frac{D(\Xi, H)}{D(R, Z)} = \frac{1}{D}\begin{bmatrix} B\cos(H) & A\sin(H) \\ -A\sin(H) & B\cos(H) \end{bmatrix}. \tag{36}$$

Then, after doing some algebra (similar to the prolate case in Sect. 3), the incompressibility constraint $\det(\mathbf{F}^{(1)}) = 1$ enforces two nonlinear ordinary differential equations for Φ_1^O and Φ_2^O, given by

$$\begin{cases} \Phi_1^O(\Phi_2^O)' - \coth^2(\Xi)(\Phi_1^O)'\Phi_2^O = 0, \\ (\Phi_1^O)^2\Phi_2 + \coth(\Xi)(\Phi_1^O)'\Phi_1^O\Phi_2^O - 1 = 0, \end{cases} \tag{37.1, 2}$$

Likewise, combining (37.1) and (37.2), it leads to

$$(\Phi_1^O)^2 = \frac{\coth(\Xi)}{\Phi_2^O\coth(\Xi) + (\Phi_2^O)'} = \Omega^O(\Xi), \qquad 2\Phi_1^O(\Phi_1^O)' = [\Omega^O(\Xi)]'. \tag{38}$$

Next, by making use of (38) and replacing $(\Phi_1^O)^2$ and $(\Phi_1^O)'$ in (37.2) by equal Φ_2^O terms, and also, defining the variable $\Psi^O(\Xi) = \Phi_2^O/(\Phi_2^O)'$, it yields

$$[\Psi^O(\Xi)]' - [\tanh^2(\Xi) + 2]\coth(\Xi)\Psi^O(\Xi) - 2\tanh^2(\Xi) - 1 = 0. \tag{39}$$

Next, Eq. (39) is integrated to give

$$\Psi^O(\Xi) = \tanh(\Xi)[C_1\cosh^2(\Xi)\sinh(\Xi) - 1]. \tag{40}$$

Finally, from Eq. (40) and using (38), the functions Φ_1^O and Φ_2^O are found to be

$$\Phi_1^O(\Xi) = \operatorname{sech}(\Xi)\left[\frac{C_1\cosh^2(\Xi)\sinh(\Xi) - 1}{C_1C_2\Upsilon_O}\right]^{\frac{1}{2}}, \tag{41}$$

$$\Phi_2^O(\Xi) = C_2\operatorname{cosech}(\Xi)\Upsilon_O, \text{ where } \Upsilon_O = \prod_{i=1}^{3}(\sinh(\Xi) - \delta_i^O)^{\frac{1+(\delta_i^O)^2}{1+3(\delta_i^O)^2}} \tag{42}$$

where C_1 and C_2 are integration constants and $\delta_i^O; i = 1, 2, 3$ are the three roots of the cubic equation $C_1(\delta^O)^3 + C_1\delta^O - 1 = 0$, given by

$$\begin{aligned} \delta_1^O &= (\sqrt[3]{12}\Gamma_O^2 - 2\sqrt[3]{18}C_1^2)/(6C_1\Gamma_O), \\ \delta_2^O &= [(\sqrt{3}i - 1)\sqrt[3]{12}\Gamma_O^2 + 2\sqrt[3]{18}(\sqrt{3}i + 1)C_1^2]/(12C_1\Gamma_O), \\ \delta_3^O &= -[(\sqrt{3}i + 1)\sqrt[3]{12}\Gamma_O^2 + 2\sqrt[3]{18}(\sqrt{3}i - 1)C_1^2]/(12C_1\Gamma_O) \end{aligned} \tag{43}$$

where $\Gamma_O = \left\{\left[9 + \sqrt{3(27 + 4C_1^2)}\right]C_1^2\right\}^{\frac{1}{3}}$. The constants C_1 and C_2 should be determined using Eq. (34), which are inherently nonlinear algebraic equations and may be solved by the Newton–Raphson method.

Concerning the associated effective energy function, the same procedure described in Sect. 4 can be followed by changing the integral representation in Eq. (23) to the oblate spheroidal coordinate system. This integral can be expressed as

$$\overline{\mathrm{W}}^O = \frac{2\pi}{V_0}\int_{\Xi_1}^{\Xi_2}\int_{-\pi/2}^{\pi/2} W^{(1)}J^O\,\mathrm{d}H\,\mathrm{d}\Xi = \int_{\Xi_1}^{\Xi_2} W^{*O}\,\mathrm{d}\Xi \tag{44}$$

where W^{*O} is the integration result of $2\pi W^{(1)} J^O / V_0$ over H, while Ξ is treated as a constant, and J^O stands for the *Jacobian* of the oblate spheroidal coordinate given by

$$J^O = \frac{C^3}{2}\cosh(\Xi)\cos(H)[\cosh(2\Xi) - \cos(2H)]. \tag{45}$$

By making use of the above relations in Sect. 4, one can finally determine the macroscopic nominal stress as given in Eq. (28). Lastly, utilizing the equations $\Xi_1 = \coth^{-1}(1/p)$, $\Xi_2 = \coth^{-1}(t^O)$, the effective strain energy $\overline{W}^O$ could be expressed as a function of the matrix material constants, Λ_1, Λ_2, p and c_0, in which $t^O = \sqrt{(Y^O)^2(1/p^2 - 1) + 1}$ and Y^O is an acceptable root of the algebraic equation $(Y^O)^3 - c_0(1 - 1/p^2)(Y^O)^2 - c_0 p^2 = 0$.

6 Numerical results and discussion

In this section, several numerical examples demonstrating the influence of the microstructure parameters on the macroscopic elastic behavior of the porous material are presented. To this end, a stored-energy function for the matrix phase should be chosen. It is noted that the kinematical model presented in Sects. 3 and 5 is quite general and could be applied for a wide variety of stored-energy functions for the matrix phase. However, for simplicity and definiteness in this section, specific results will be presented and discussed for porous materials with an isotropic neo-Hookean matrix characterized by the energy potential of the form

$$W^{(1)} = \frac{1}{2}\mu^{(1)}(I_1 - 3) \tag{46}$$

where $\mu^{(1)}$ is the ground-state shear modulus. For the case here, the double integration expressed in Eqs. (23) and (44) can be performed first over the angle H from which an analytical expression is obtained, which can be simplified to

$$\begin{aligned} W^{*P} = {} & \frac{1}{2}\mu^{(1)}\sqrt{[1 - 1/(t^P)^2]}[(t^P)^2 - 1]\sinh(\Xi)\Big\{[3\cosh^2(2\Xi) - 1][2(\Phi_1^P(\Xi))^2 + (\Phi_2^P(\Xi))^2] \\ & + \sinh(2\Xi)[2\Phi_1^P(\Xi)\Theta_2^P(\Xi) + \Phi_2^P(\Xi)\Theta_1^P(\Xi)] + 2\sinh^2(\Xi)(\Theta_2^P(\Xi))^2 \\ & + \cosh^2(\Xi)(\Theta_1^P(\Xi))^2 - 9\cosh^2(\Xi) + 3\Big\}, \end{aligned} \tag{47}$$

$$\begin{aligned} W^{*O} = {} & \frac{1}{2}\mu^{(1)}[1 - 1/(t^O)^2]\sqrt{(t^O)^2 - 1}\cosh(\Xi)\Big\{[3\cosh(2\Xi) - 1](\Phi_1^O(\Xi))^2 + 2\sinh(2\Xi)\Phi_1^O(\Xi)\Theta_2^O(\Xi) \\ & + 2\cosh^2(\Xi)\Theta_2^O(\Xi)^2 + [3\cosh^2(\Xi) - 2]\Phi_2^2(\Xi) \\ & + [\sinh(2\Xi)\Phi_2^O(\Xi) + \sinh^2(\Xi)](\Theta_1^O(\Xi))^2 - 9\cosh^2(\Xi) + 6\Big\}, \end{aligned} \tag{48}$$

respectively, for prolate and oblate voids. For the sake of continuity, the derivation of functions $\Theta_1^{O,P}(\Xi)$ and $\Theta_2^{O,P}(\Xi)$ is given in "Appendix A". Next, for integrating with respect to variable Ξ, it is convenient to utilize the Gaussian quadrature formula as follows:

$$\overline{W} = \sum_{i=1}^{\infty} M_i N_i^2 W^*|_{\Xi_i = N_i}, \tag{49}$$

where the weights M_i and nodal abscissas N_i are computed with a high precision for a large number of nodes. The remainder of this section is devoted to compare the stress–strain curves derived by using the presented model with the corresponding finite element results. Here, it is worth mentioning that the results for the macroscopic response of porous materials whose matrix phase is characterized by the functional form $W^{(1)}(I_1, I_2)$ (including neo-Hookean form) are not proper candidates to be verified with corresponding experimental data. This observation (reported by Criscione [27]) (for homogenous materials) is due to the fact that the experimental error which is inherent in tests on real materials is magnified when the functional form of $W^{(1)}(I_1, I_2)$ is assumed for the material a priori. However, it is emphasized that the presented kinematical formulation is capable to generate the results for porous materials whose matrix phase is governed by (experimentally) well-posed stored-energy functions, such as the Ogden energy function [28].

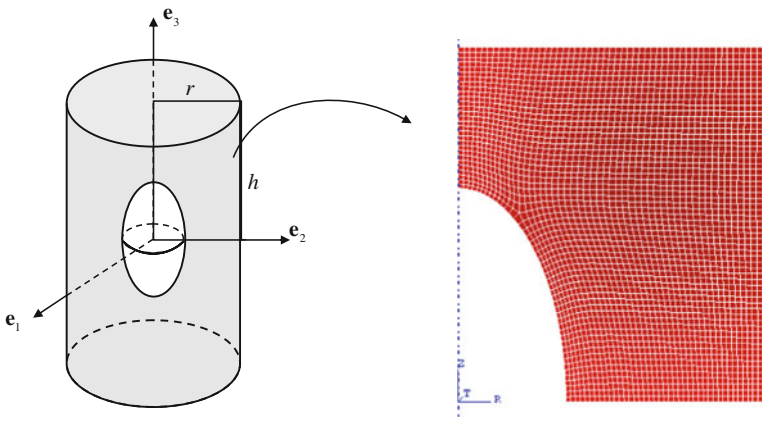

Fig. 2 An axisymmetric unit cell for finite element modeling

6.1 Comparison with finite element results

In this subsection, we perform a comparison between the results of the semi-analytical model presented in the previous sections with the corresponding results of a finite element (FE) simulation for the class of porous materials under study. For a complete simulation of the actual microstructure shown in Fig. 1a, a three-dimensional FE model consisting of randomly distributed voids is required. However, from a computational point of view, this model would be very intensive. The basic feature of the structure and its behavior can be approximately idealized by a circular cylindrical cell of radius r and length h in whose center an aligned spheroidal void of volume fraction c_0 and aspect ratio p is embedded (see Fig. 2). Such a unit cell has been extensively used for numerical modeling of porous materials with spheroidal voids [22,23,29] to compute the overall properties of the materials, particularly in the field of *Metal Matrix Porous* materials. In fact, this unit cell represents an elementary cell in a lattice with hexagonal array of voids [30] whose specific void arrangement can macroscopically capture the major effects of void–void interactions.

The uniform normal displacement is enforced on the top surface of the unit cell, and the normal displacement on the lateral surface is also prescribed to preserve the cylindrical geometry of the unit cell during the whole loading. The behavior of the cell model is considered for two specific axisymmetric loading cases: (i) 3-D hydrostatic tension and (ii) plane strain hydrostatic tension. The affine boundary conditions are expressed in terms of the macroscopic deformation gradient $\overline{\mathbf{F}}$ for each case. In order to examine the influence of the microstructural variables on the macroscopic state of stress, we consider, in our analysis, a relatively wide range of void aspect ratios and two values for initial porosity. The selected initial porosities and aspect ratios are taken to be $c_0 = 0.15, 0.25$ and $p = 2, 5, 10$ (for the oblate voids, the corresponding aspect ratios are $p = 0.5, 0.2, 0.1$). The finite element calculations have been carried out by the ABAQUS 6.5 package in which quadrature isoparametric elements providing a parabolic displacement field have been used. Results of FE are shown by markers and labeled with FEM, and those of the present analytical model are depicted by lines and labeled with ASM (assemblage model). Results of calculations for the two cases of loading are presented in the following subsections.

6.1.1 3-D hydrostatic tension

Upon applying the macroscopic deformation gradient $\overline{\mathbf{F}} = \mathrm{diag}(\Lambda_1, \Lambda_1, \Lambda_1)$, the anisotropic growth of voids occurs, and it has been taken into account by the constitutive model (Eq. 28). The variations of the macroscopic stress components $\overline{S}_{11}(=\overline{S}_{rR})$ and $\overline{S}_{33}(=\overline{S}_{zZ})$, as functions of the macroscopic volume change $\ln \overline{J} = 3 \ln \Lambda_1$, for two values of the initial porosities and three different initial aspect ratios are shown in Figs. 3 and 4 corresponding to the oblate and prolate shapes of the voids, respectively. The results are normalized by the ground-state shear moduli ($\mu^{(1)} = 1$). A comparison between the results of FEM and those of the present analytical model shows a good agreement for a variety of aspect ratios and the chosen porosities. However, in the case of oblate voids, the lines associated with component $\overline{S}_{33}$ and for prolate voids, those lines associated with both stress components lie slightly below the corresponding markers. This indicates a minor underestimation in the results associated with the analytical model in contrast to those of the FEM results. Also, it is observed

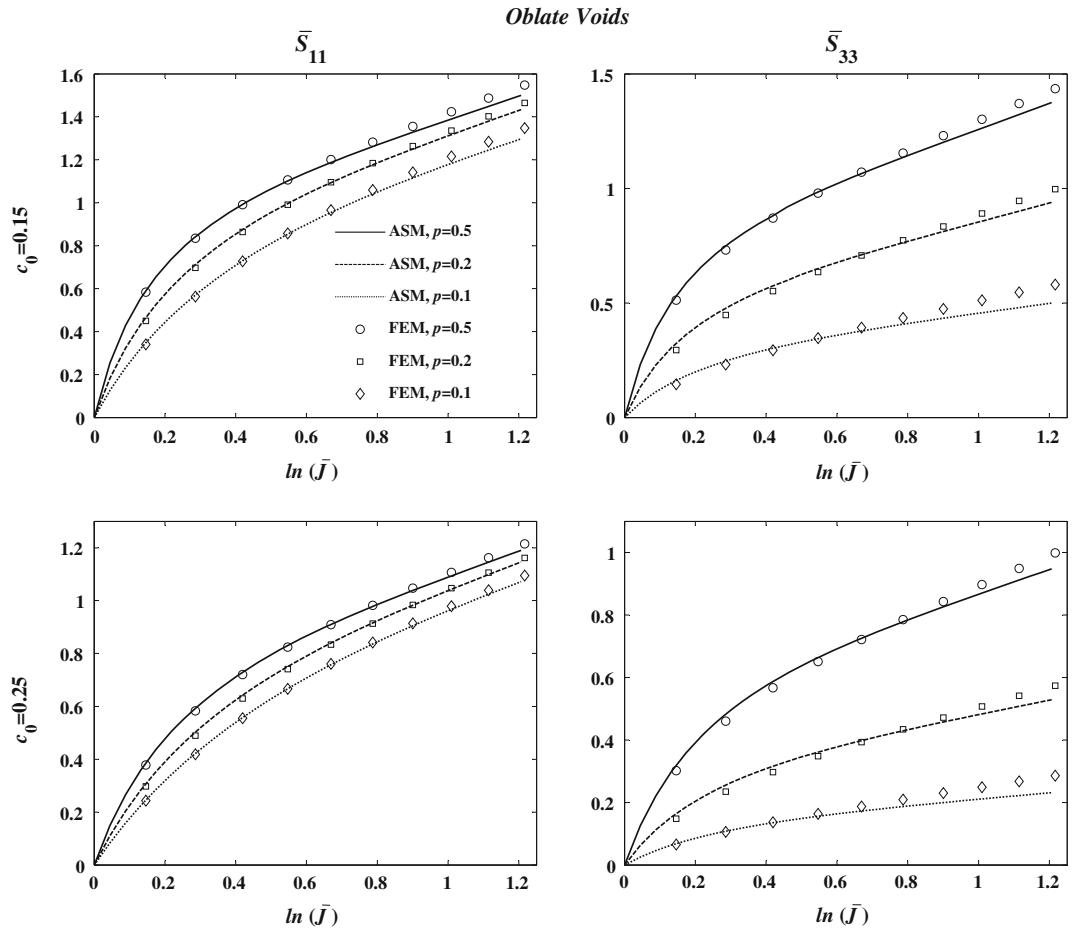

Fig. 3 Variation of macroscopic nominal stresses with macroscopic stretch under hydrostatic loading for an elastomer containing unidirectional oblate voids. *Markers* indicate FE simulation results, and *lines* refer to the results of the present analytical work .

from Figs. 3 and 4 that, for a given porosity, as the initial shape of voids tends to a disk-like ($p \to 0$) or needle-like ($p \to \infty$) shape, the porous material exhibits a softer effective behavior. However, it is noticed from Fig. 4 that the results for the porous material with prolate voids (specifically the results for the component $\overline{S}_{33}$) are comparatively less sensitive to the aspect ratio of the voids. Moreover, it is worth mentioning that, in the special case of spherical voids ($p = 1$), the analytical results under hydrostatic tension will reduce to analytical results of Hashin [12] for a neo-Hookean matrix.

6.1.2 Axisymmetric plane strain tension

The capacity of the current solution in describing the nonlinearity of the in-plane hydrostatic tension is demonstrated herein by applying a macroscopic deformation distinguished by $\overline{\mathbf{F}} = \text{diag}(\Lambda_1, \Lambda_1, 1)$. Noting that the out-of-plane direction is aligned with the symmetry axis $\mathbf{e}_3$, the effective stress calculation is done by Eqs. (28), (29), (30) and (49). A schematic representation of the (axisymmetric) FE unit cell containing a disk-like void (oblate void with $p = 0.1$) in the deformed configuration is depicted in Fig. 5. The calculations for the macroscopic stress component $\bar{S}_{11}$ versus the macroscopic principle stretch Λ_1 are shown in Figs. 6 and 7, respectively, corresponding to the oblate and prolate shapes of the voids. As far as the curves of Figs. 6 and 7 are concerned, we observe that the results of FE, shown by markers, and the theoretical approach, shown by lines, are in a good agreement with each other. Similar to the results for 3-D hydrostatic tension, the stress component associated with the porous material with prolate voids is again less sensitive to the aspect ratio of the voids.

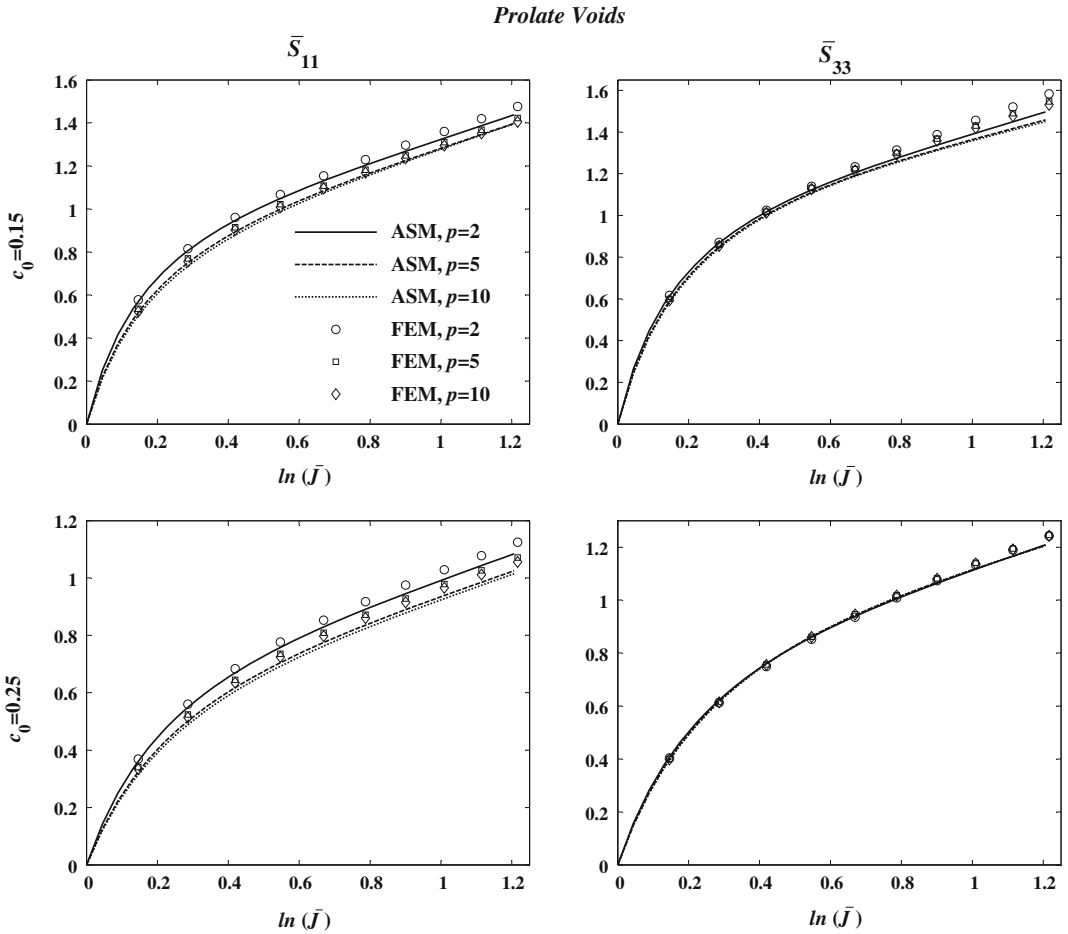

Fig. 4 Variation of macroscopic nominal stresses with macroscopic stretch under hydrostatic loading for an elastomer containing unidirectional prolate voids. *Markers* indicate FE simulation results, and *lines* refer to the results of the present analytical work

Fig. 5 Deformed shape of the unit cell with a disk-like cavity

7 Conclusion

The aim of this work was to develop a constitutive model for porous elastomers consisting of randomly dispersed, unidirectionally aligned spheroidal voids in an incompressible matrix. The model was aimed to account for both void shape effects and influence of void concentration. Both prolate and oblate shapes of spheroidal voids were studied. The reliability of the model was evaluated by comparing its predictions with the corresponding FEM results, obtained by micromechanical simulations of a simple RVE comprising of a cylindrical cell with an enclosed spheroidal void. The results were calculated for macroscopic stress–deformation behaviors, and attention was focused on axisymmetric loadings and some selected void aspect ratios and volume fractions. It was shown that the results of the present model are in a fairly good agreement with the corresponding FEM results both qualitatively and quantitatively. It was also observed that the macroscopic stress components associated with the porous elastomers with prolate voids' are less sensitive to the voids' aspect ratio. Lastly, it is noteworthy to remark that this model can be extended for more general loadings; however, an exact solution to a proposed trial field might not be available.

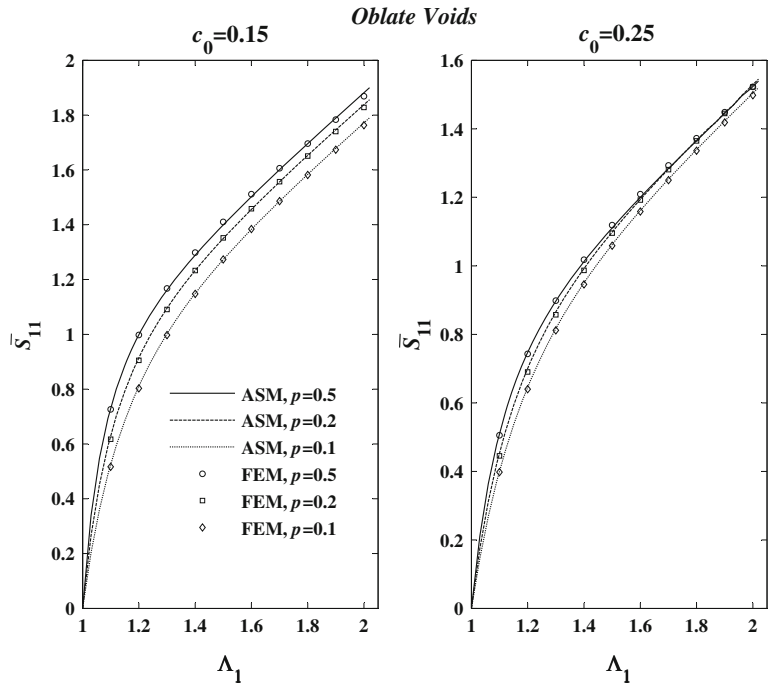

Fig. 6 Variation of macroscopic nominal stresses with macroscopic stretch under axisymmetric plane strain loading for an elastomer containing unidirectional oblate voids. *Markers* indicate FE simulation results, and *lines* refer to the results of the present analytical work

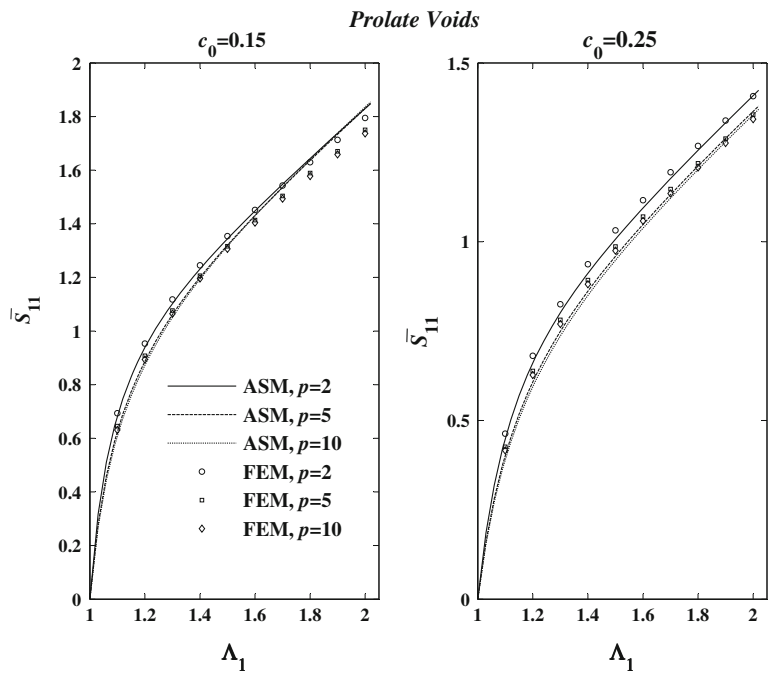

Fig. 7 Variation of macroscopic nominal stresses with macroscopic stretch under axisymmetric plane strain loading for an elastomer containing unidirectional prolate voids. *Markers* indicate FE simulation results, and *lines* refer to the results of the present analytical work

Appendix A

In this Appendix, we provide the expressions for $\Theta_1^{O,P}(\Xi)$ and $\Theta_2^{O,P}(\Xi)$ used in Eqs. (47) and (48). They are given by

$$\Theta_1^P(\Xi) = \Phi_2^P(\Xi)\left\{\sinh(\Xi)\sum_{i=1}^{3}\frac{(\delta_i^P)^2-1}{[\cosh(\Xi)-\delta_i^P][3(\delta_i^P)^2-1]} - \tanh(\Xi)\right\}, \tag{A.1}$$

$$\Theta_2^P(\Xi) = -\frac{[(2\tanh^2(\Xi)-1)\Theta_1^P(\Xi)+\tanh(t)\Theta_3^P(\Xi)]}{2[\tanh(\Xi)\Phi_2^P(\Xi)+\Theta_1^P(\Xi)]^2\sqrt{\tanh(\Xi)/[\tanh(\Xi)\Phi_2^P(\Xi)+\Theta_1^P(\Xi)]}} \tag{A.2}$$

for prolate voids, where

$$\Theta_3^P(\Xi) = \Phi_2^P(\Xi)\left\{\left\{\tanh(\Xi)-\sinh(\Xi)\sum_{i=1}^{3}\frac{(\delta_i^P)^2-1}{[\cosh(\Xi)-\delta_i^P][3(\delta_i^P)^2-1]}\right\}^2 -1+\tanh^2(\Xi)+[\cosh(\Xi)-\sinh^2(\Xi)]\sum_{i=1}^{3}\frac{(\delta_i^P)^2-1}{[\cosh(\Xi)-\delta_i^P][3(\delta_i^P)^2-1]}\right\}, \tag{A.3}$$

and

$$\Theta_1^O(\Xi) = \Phi_2^O(\Xi)\left\{\cosh(\Xi)\sum_{i=1}^{3}\frac{1+(\delta_i^O)^2}{[\sinh(\Xi)-\delta_i^O][1+3(\delta_i^O)^2]} - \coth(\Xi)\right\}, \tag{A.4}$$

$$\Theta_2^O(\Xi) = -\frac{[(2\coth^2(\Xi)-1)\Theta_1^O(\Xi)+\coth(t)\Theta_3^O(\Xi)]}{2[\coth(\Xi)\Phi_2^O(\Xi)+\Theta_1^O(\Xi)]^2\sqrt{\coth(\Xi)/[\coth(\Xi)\Phi_2^O(\Xi)+\Theta_1^O(\Xi)]}} \tag{A.5}$$

for oblate voids, where

$$\Theta_3^O(\Xi) = \Phi_2^O(\Xi)\left\{\left\{\coth(\Xi)-\cosh(\Xi)\sum_{i=1}^{3}\frac{1+(\delta_i^O)^2}{[\sinh(\Xi)-\delta_i^O][1+3(\delta_i^O)^2]}\right\}^2 -1+\coth^2(\Xi)+[\sinh(\Xi)-\cosh^2(\Xi)]\sum_{i=1}^{3}\frac{1+(\delta_i^O)^2}{[\sinh(\Xi)-\delta_i^O][1+3(\delta_i^O)^2]}\right\}. \tag{A.6}$$

References

1. Nemat-Nasser, S., Hori, M.: Micromechanics: Overall Properties of Heterogeneous Solids. Elsevier, Amsterdam (1993)
2. Milton, G.W.: The Theory of Composites. Cambridge University Press, Cambridge (2002)
3. Buryachenko, V.: Micromechanics of Heterogeneous Materials. Springer, Berlin (2007)
4. Danielsson, M., Parks, D.M., Boyce, M.C.: Constitutive modeling of porous hyperelastic materials. Mech. Mater. **36**, 347–358 (2004)
5. Lopez-Pamies, O., Ponte Castaneda, P.: Homogenization-based constitutive models for porous elastomers and implications for macroscopic instabilities: II—results. J. Mech. Phys. Solids **55**, 1702–1728 (2007)
6. Bucknall, CB.: Toughened Plastics. Applied Science, London (1977)
7. Talbot, D.R.S., Willis, J.R.: Variational principles for inhomogeneous non-linear media. IMA J. Appl. Math. **35**, 39–54 (1985)
8. Ponte Castaneda, P.: Second-order homogenization estimates for nonlinear composites incorporating field fluctuations. I. Theory. J. Mech. Phys. Solids **50**, 737–757 (2002)
9. Lopez-Pamies, O., Ponte Castaneda, P.: Homogenization-based constitutive models for porous elastomers and implications for macroscopic instabilities: I—analysis. J. Mech. Phys. Solids **55**, 1677–1701 (2007)
10. Hashin, Z.: The elastic moduli of heterogeneous materials. J. Appl. Mech. **29**, 43–50 (1962)
11. Hashin, Z., Rosen, B.: The elastic moduli of fiber reinforced materials. J. Appl. Mech. **31**, 223–32 (1964)
12. Hashin, Z.: Large isotropic elastic deformation of composites and porous media. Int. J. Solids Struc. **21**, 711–720 (1985)
13. Kakavas, PA., Anifantis, N.K.: Effective moduli of hyperelastic porous media at large deformation. Acta Mech. **160**, 127–147 (2003)

14. deBotton, G., Hariton, I., Socolsky, E.A.: Neo-Hookean fiber-reinforced composites in finite elasticity. J. Mech. Phys. Solids **54**, 533–559 (2006)
15. deBotton, G., Hariton, I.: Out-of-plane shear deformation of a neo-hookean fiber composite. Phys. Lett. A **354**, 156–60 (2006)
16. Avazmohammadi, R., Naghdabadi, R.: Strain energy-based homogenization of non-linear elastic particulate composites. Int. J. Eng. Sci. **47**, 1038–1048 (2009)
17. Avazmohammadi, R., Naghdabadi, R., Weng, G.J.: Finite anti-plane shear deformation of nonlinear composites reinforced by elliptic fibers. Mech. Mater. **41**, 868–877 (2009)
18. Goudarzi, T., Lopez-Pamies, O.: Numerical modeling of the nonlinear elastic response of filled elastomers via composite-sphere assemblages. J. Appl. Mech. (2013) (in press)
19. Zhao, Y.H., Tandon, G.P., Weng, G.J.: Elastic moduli for a class of porous materials. Acta. Mech. **76**, 105–131 (1989)
20. Bouchart, V., Brieu, M., Kondo, D., Nait Abdelaziz, M.: Implementation and numerical verification of a non-linear homogenization method applied to hyperelastic composites. Comput. Mater. Sci. **43**, 670–680 (2008)
21. Benveniste, Y., Milton, G.W.: New exact results for the effective electric, elastic, piezoelectric and other properties of composite ellipsoid assemblages. J. Mech. Phys. Solids **51**, 1773–1813 (2003)
22. Gologanu, M., Leblond, J.-B., Devaux, J.: Approximate models for ductile metals containing non-spherical voids-case of axisymmetric prolate ellipsoidal cavities. J. Mech. Phys. Solids. **41**, 1723–1754 (1993)
23. Gologanu, M., Leblond, J.B., Devaux, J.: Approximate models for ductile metals containing nonspherical voids-case of axisymmetric oblate ellipsoidal cavities. J. Eng. Mater. Tech. Trans. ASME **116**, 290–297 (1994)
24. Hou, H., Abeyaratne, R.: Cavitation in elastic and elastic–plastic solids. J. Mech. Phys. Solids **40**, 571–592 (1992)
25. Hill, R.: On constitutive macro-variables for heterogeneous solids at finite strain. Proc. R. Soc. Lond. Ser. A Math. Phys. Sci. **326**, 131–147 (1972)
26. Criscione, J.C., Douglas, A.S., Hunter, W.C.: Physically based strain invariant set for materials exhibiting transversely isotropic behavior. J. Mech. Phys. Solids **49**, 871–897 (2001)
27. Criscione, J.C.: Rivlin's representation formula is ill-conceived for the determination of response functions via biaxial testing. J. Elast. **70**, 129–147 (2003)
28. Ogden, R.W.: Nonlinear Elastic Deformations. Halsted Press, New York (1984)
29. Siruguet, K., Leblond, J.B.: Effect of void locking by inclusions upon the plastic behavior of porous ductile solids—I: theoretical modeling and numerical study of void growth. Int. J. Plast. **20**, 225–254 (2004)
30. Li, Y., Ramesh, K.T.: Influence of particle volume fraction, shape, and aspect ratio on the behavior of particle-reinforced metal matrix–matrix composites at high rates of strain. Acta. Mater. **46**, 5633–5646 (1998)